

# Residue-Enhanced Pion–Rho Mixing as the Origin of Nonmonotonic Charged Pion Mass in Magnetic Fields

Ziyue Wang

*School of Physics and Optoelectronic Engineering,  
Beijing University of Technology, Beijing 100021, China*

(Dated: February 18, 2026)

We identify the dynamical origin of the non-monotonic magnetic-field dependence of the charged pion mass observed in lattice QCD. Using a near-pole effective action derived from the SU(2) Nambu–Jona-Lasinio model, we show that the lowest-Landau-level charged pion mixes with the longitudinally polarized charged rho meson, which shares the same quantum numbers in a magnetic background. This mixing, generated by quark-loop polarization and a gauge-invariant tree-level operator matched to the vacuum decay  $\rho^\pm \rightarrow \pi^\pm \gamma$ , induces strong level repulsion. Crucially, this effect is dynamically amplified by a rapid suppression of the rho-meson wave-function renormalization near the pole. As a result, the lower eigenmode exhibits a turnover as the magnetic field increases. The mechanism is analogous to singlet–triplet mixing in positronium and provides a natural explanation for the lattice results. Such effects are expected to be generic for charged mesons in magnetic fields when symmetry-allowed mixing and near-pole residue suppression are present.

*Introduction.* Strong magnetic fields, reaching up to  $10^{19}$  Gauss ( $|eB| \sim 10m_\pi^2$ ) realized in a variety of physical environments, including the early universe, magnetars, and non-central heavy-ion collisions [1–5] can significantly influence the behavior of QCD matter [6–14]. Comprehensive reviews of QCD in strong magnetic fields can be found in Refs. [15–17]. At such intensities, magnetic-field–induced QED effects become comparable to hadronic scales and can qualitatively modify both the phase structure of QCD matter and the properties of QCD bound states. In particular, the spectrum of charged mesons is strongly affected: their transverse motion is quantized into Landau levels, while their internal structure can be significantly distorted by the magnetic field.

Recent lattice QCD simulations have focused on the QCD properties in magnetic field [11, 18, 19] and revealed an unexpected feature of charged mesons [20–22]: the effective mass of the charged pion exhibits a non-monotonic dependence on the magnetic field strength. While the mass initially increases at weak fields, consistent with the lowest-Landau-level expectation, it reaches a maximum at intermediate fields and subsequently decreases as the field is further increased. This behavior cannot be explained by Landau quantization alone and has remained a long-standing discrepancy between lattice results and model descriptions.

Meson properties in magnetic fields have been intensively investigated in effective models and continuum approaches [23–31], including NJL-type models, functional methods, and holographic descriptions. More recent studies have attempted to account for the lattice behavior by incorporating magnetic-field–dependent quark couplings [32], meson mixing effects [33, 34], wave-function renormalization [35], or inverse magnetic catalysis [36]. However, none of these approaches has been able to reproduce the lattice trend in a fully satisfactory manner, suggesting that an additional dynamical mechanism becomes operative at strong magnetic fields.

Vector mesons in magnetic backgrounds, in particular the charged  $\rho$ , have also been studied extensively [37–39], where modifications of polarization structure and possible condensation phenomena were discussed. In this Letter, we demonstrate the non-monotonic behavior is a direct consequence of magnetic-field–induced mixing between the lowest-Landau-level charged pion  $\pi^+$  and the longitudinally polarized charged rho meson  $\rho_{s_z=0}^+$ . In a magnetic background, these two modes share the same conserved quantum numbers, allowing them to mix in close analogy with singlet–triplet mixing in positronium. Using a near-pole effective action derived from the SU(2) Nambu–Jona-Lasinio model [40–42], we show that this mixing leads to strong level repulsion.

Crucially, the effect is dynamically amplified by a rapid suppression of the wave-function renormalization of the longitudinal rho mode near the pole. As a consequence, the lower eigenmode bends downward at large magnetic fields, naturally producing the turnover observed in lattice QCD. Since lattice simulations extract an effective mass from the long-time behavior of charged-pion correlators, we demonstrate that the relevant theoretical observable is the lowest near-pole eigenmode, rather than the unmixed pion Landau level. More generally, our results highlight that residue effects—often neglected in phenomenological analyses—can qualitatively reshape the charged-meson spectrum in strong magnetic fields. This mechanism is expected to be universal for charged mesons whenever magnetic-field–induced mixing between modes with identical quantum numbers is present.

*Effective near-pole description.* To treat  $\pi^+$  and  $\rho^+$  as quark–antiquark bound states on equal footing and to describe their magnetic-field–induced mixing consistently, we derive the quadratic bosonic action from a microscopic quark theory in a uniform external magnetic field. Projecting the resulting inverse propagator onto mesonic Landau eigenstates yields a Landau-level–resolved kernel that contains the full energy dependence inherited from the quark loop.

The low-energy dynamics relevant for lattice observables is governed by the lowest Landau level (LLL), rather than by rest masses alone. Instead of solving the full Landau-projected kernel directly, we construct a controlled near-pole effective description for the LLL by expanding the diagonal elements around their respective poles and canonically normalizing the fields. This procedure isolates the relevant collective modes and makes the dynamical role of residues and mixing terms transparent.

After canonical normalization, the LLL dynamics in the closed subspace of  $\pi^+$  and longitudinal  $\rho_{s_z=0}^+$  is captured by the near-pole quadratic kernel

$$\mathcal{K}_c(q_0) \approx \begin{pmatrix} q_0^2 - E_\pi^2(B) & -iq_0 h(B) \\ iq_0 h(B) & q_0^2 - E_\rho^2(B) \end{pmatrix}, \quad (1)$$

where  $E_\pi(B)$  and  $E_\rho(B)$  are the unmixed lowest-Landau-level energies of the pion and longitudinal rho meson, respectively. The physical eigenmodes within this near-pole effective theory are obtained from the pole condition

$$\det \mathcal{K}_c(q_0) = 0. \quad (2)$$

This procedure assumes that the relevant collective mode remains adiabatically connected to the unmixed lowest-Landau-level pole, an assumption whose validity can be tested by comparison with the full Landau-projected kernel introduced below.

The diagonal entries are defined by the near-pole expansion of the corresponding Landau-projected kernels,

$$K_{\phi\phi} \simeq Z_\phi(B)(q_0^2 - E_\phi^2(B)), \quad \phi = \pi, \rho. \quad (3)$$

This expansion is performed directly at the Landau-projected pole, ensuring that the effective theory captures the collective excitation measured in lattice correlators. The wave-function renormalizations  $Z_\pi(B)$  and  $Z_\rho(B)$  at the pole encode the sensitivity of each mode to the magnetic background and play a central role in the mixing dynamics.

The off-diagonal terms describe magnetic field induced mixing between the pion and the longitudinal rho mode. Their strength is parametrized as

$$h(B) = \frac{eB[g_{\rho\pi}^{\text{loop}}(B) + g_{\rho\pi}^{\text{tree}}]}{\sqrt{Z_\pi(B)Z_\rho(B)}}. \quad (4)$$

Here  $g_{\rho\pi}^{\text{loop}}(B)$  arises from quark-loop polarization in the magnetic field, while  $g_{\rho\pi}^{\text{tree}}$  denotes a gauge-invariant local coupling fixed by the vacuum decay  $\rho^\pm \rightarrow \pi^\pm \gamma$ . The explicit factor of  $eB$  reflects the magnetic origin of the mixing, while the inverse square root of the residues implies a dynamical enhancement when the wave-function renormalization becomes small.

The structure of the kernel makes the physical mechanism transparent: as the magnetic field increases, the mixing induces level repulsion between a light pion mode  $\pi^+$  and a heavier longitudinal rho mode  $\rho_{s_z=0}^+$ . When

the residue  $Z(B)$  decreases rapidly, the effective mixing strength  $h(B)$  is strongly amplified near the pole, leading to a downward bending of the lower eigenmode. This residue-enhanced level repulsion provides a natural route to non-monotonic magnetic-field dependence of the charged pion energy.

*Microscopic origin* We now derive the ingredients entering the near-pole effective kernel directly from the underlying quark dynamics in a magnetic field. In particular, the unmixed energies  $E_\pi(B)$ ,  $E_\rho(B)$ , the wavefunction renormalizations  $Z_\pi(B)$ ,  $Z_\rho(B)$ , and the loop-induced mixing  $g_{\rho\pi}^{\text{loop}}(B)$  are obtained from Landau-level-projected quark polarization functions. We evaluate these quantities within the SU(2) Nambu–Jona–Lasinio model with quarks minimally coupled to the background field  $\mathcal{L} = \bar{\psi}(iD^\mu - m_0)\psi + G_S[(\bar{\psi}\psi)^2 + (\bar{\psi}i\gamma^5\psi)^2] - G_V[(\bar{\psi}\gamma^\mu\tau^a\psi)^2]$ , with  $\tau^a$  representing the isospin Pauli matrices, and  $G_S$  and  $G_V$  the coupling constants with respect to the scalar (pseudoscalar) and the vector channels [40–42]. The covariant derivative couples quarks to an external magnetic field  $\vec{B} = B\hat{z}$  along the positive  $z$  direction. For the quark propagator we use Landau-level representations [15, 43].

After Hubbard–Stratonovich transformation, integrating out the quark fields, and expanding to quadratic order generates a matrix of polarization functions for the charged pion and rho channels,

$$S_{\text{eff}}^{(2)} = \frac{1}{2} \int d^4x d^4y \Phi^\dagger(x) [\mathcal{G}^{-1}\delta(x-y) - \Pi(x,y)]\Phi(y) + S_{\text{tree}}^{(2)}, \quad (5)$$

where we restrict to the reduced subspace of  $\pi^+$  and  $\rho_{s_z=0}^+$  denoted by  $\Phi = (\pi, \rho_3)^T$ ,  $\mathcal{G}^{-1} = \text{diag}(1/2G_S, 1/2G_V)$  is the contact inverse propagator, and  $\Pi$  is the polarization matrix from the quark loop.  $S_{\text{tree}}^{(2)}$  comes from the gauge-invariant tree-level counterterm

$$S_{\text{tree}}^{(2)} = \int d^4x \kappa_{\rho\pi}^{\text{tree}} (\rho_\mu^+ \tilde{F}^{\mu\nu} D_\nu \pi^- + \rho_\mu^- \tilde{F}^{\mu\nu} D_\nu \pi^+). \quad (6)$$

To focus ourselves on the given Landau level modes in the bosonic action, we expand the meson field by their eigenfunctions in magnetic field

$$\phi(x) = \sum_{n, q_y, q_z} \phi_n(q_0, q_3) \varphi_n(x_\perp) e^{-iq_0 t + iq_3 z} \quad (7)$$

with  $\phi$  stands for  $\pi^+$  or the longitudinal  $\rho^+$ , and  $\varphi_n$  is the standard gauge dependent Landau wavefunctions. Because u and d quarks carry different electric charges, the polarization functions acquire nontrivial Schwinger phases. Upon projection onto charged-meson Landau eigenstates, these phases combine with the external wave functions to produce gauge-invariant Landau-projected kernels. Landau quantization therefore enters both through internal quark propagators and external meson legs, and their combined structure determines the

magnetic-field dependence of the meson spectrum. Then the boson quadratic action (5) becomes a sum over Landau levels:

$$S_{\text{eff}}^{(2)} = \frac{1}{2} \sum_n \int \frac{dq_0}{2\pi} \Phi_n^\dagger(q_0) \mathcal{K}(q_0; B, n) \Phi_n(q_0), \quad (8)$$

with  $\Phi_n = (\pi_n, \rho_n)^T$  is the subspace of  $\pi^+$  and  $\rho_{s_z=0}^+$  at given Landau level  $n$ . Projecting the quadratic bosonic action onto mesonic Landau eigenstates yields the microscopic Landau-level-projected inverse propagator,

$$\mathcal{K}(q_0; B, n) = \begin{pmatrix} \mathcal{K}_{\pi\pi}(q_0; B, n) & \mathcal{K}_{\pi\rho}(q_0; B, n) \\ \mathcal{K}_{\rho\pi}(q_0; B, n) & \mathcal{K}_{\rho\rho}(q_0; B, n) \end{pmatrix}, \quad (9)$$

with  $\mathcal{K}_{\pi\pi} = \frac{1}{2G_S} - \Pi_{\pi\pi, n}(q_0, B)$ ,  $\mathcal{K}_{\rho\rho} = \frac{1}{2G_V} - \Pi_{\rho\rho, n}(q_0, B)$ ,  $\mathcal{K}_{\rho\pi} = -\Pi_{\rho\pi, n}^3(q_0, B) + \mathcal{K}_{\rho\pi}^{\text{tree}}(q_0, B)$ ,  $\mathcal{K}_{\pi\rho} = -\Pi_{\pi\rho, n}^3(q_0, B) + \mathcal{K}_{\pi\rho}^{\text{tree}}(q_0, B)$ , and the Landau projected polarization function is defined as  $\Pi_{\phi_1\phi_2, n}(q_0, B) = \int d^4x d^4y \varphi_n^*(x) \Pi_{\phi_1\phi_2}(x, y; B) \varphi_n(y)$ . This Landau-level-projected kernel contains the full energy dependence inherited from the quark loop and does not rely on any near-pole expansion. Solving  $\det \mathcal{K}(q_0; N, n=0) = 0$  directly therefore yields the complete determinant spectrum within the NJL model, providing a reference against which the near-pole reduction can be assessed.

The unmixed lowest-Landau-level energies  $E_\pi(B)$  and  $E_\rho(B)$  are defined by the pole conditions of the diagonal Landau-projected kernels,

$$\begin{aligned} \mathcal{K}_{\pi\pi}(q_0 = E_\pi; B, n=0) &= 0, \\ \mathcal{K}_{\rho\rho}(q_0 = E_\rho; B, n=0) &= 0. \end{aligned} \quad (10)$$

These pole conditions define the unmixed LLL energies. The corresponding wave-function renormalizations are determined from the slopes of the diagonal kernels at the poles,  $Z_\phi(B) = \partial \mathcal{K}_{\phi\phi}(q_0; B, n=0) / \partial q_0^2|_{q_0^2=E_\phi^2(B)}$ . The near-pole kernel in (1) is obtained by expanding this microscopic Landau-projected kernel around the LLL poles and retaining the leading energy dependence relevant for the collective modes.

The off-diagonal kernel arises from mixed quark-loop polarization between the pseudoscalar and vector channels. In a magnetic field, this contribution is nonvanishing for the longitudinal rho mode and takes the generic form

$$\Pi_{\rho\pi}^3(q_0, B) = -iq_0 e B g_{\rho\pi}^{\text{loop}}(B) \quad (11)$$

as well as  $\Pi_{\pi\rho}^3 = \Pi_{\rho\pi}^{3*}$ . The explicit  $q_0$  factor follows from the Dirac trace structure and ensures that mixing vanishes in the static limit, consistent with parity. This directly generates the loop-induced component of the mixing strength defined in the effective theory (1). In the absence of a magnetic field, Lorentz and parity symmetries forbid such mixing, and the corresponding polarization function vanishes identically.

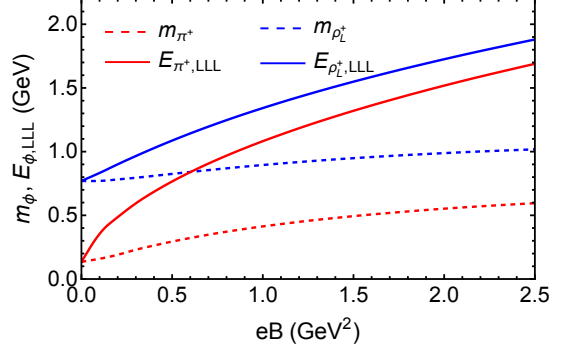


FIG. 1: Unmixed lowest-Landau-level (LLL) energies  $E_\pi(B)$  and  $E_\rho(B)$  obtained from the diagonal Landau-projected kernels (10), together with the corresponding rest masses  $m_\phi = \sqrt{E_\phi^2 - eB}$ . Both unmixed LLL energies increase monotonically with the magnetic field.

In addition to the loop contribution, the gauge-invariant local operator (6) encodes short-distance physics and reproduces the observed vacuum decay  $\Gamma_{\text{exp}}(\rho^\pm \rightarrow \pi^\pm \gamma) \approx 0.068$  MeV. The coefficient of this operator is fixed by matching to the experimental partial width in vacuum, yielding a field-independent contribution  $g_{\rho\pi}^{\text{tree}} = 0.112$  GeV $^{-1}$  to the effective mixing strength. Together, the loop-induced and tree-level contributions fully determine the magnetic-field dependence of the mixing in the near-pole kernel.

After canonical normalization, the LLL dynamics of  $\pi^+$  and  $\rho_{s_z=0}^+$  system is captured by the near-pole quadratic kernel (1), with the explicit Landau projected polarization functions are included in the appendix A. The pole condition  $\det \mathcal{K}_c(q_0) = 0$  produces two eigenmodes, in the following we focus on the lower band. In practice, we use (1) for the near-pole analysis and (9) for the direct determinant solution shown in Fig.4.

**Results** In the calculation, we use the Pauli Villars regulation with three regulators  $a_i = \{0, 1, 2, 3\}$ ,  $c_i = \{1, -3, 3, -1\}$ . The model parameters are chosen to be  $\Lambda = 1.2$  GeV,  $G_S = 3.72$  GeV $^{-2}$ ,  $G_V = 5.76$  GeV $^{-2}$ . These parameters correspond to  $m_\pi = 0.135$  GeV,  $m_\rho = 0.77$  GeV. The summation of Landau level is performed to over 200 Landau levels, which is sufficient for the range of magnetic field considered. The NJL mean field gap equation reproduce the magnetic catalysis at  $T = 0.01$  GeV as expected in lattice and other model analysis.

We first determine the unmixed lowest-Landau-level (LLL) energies of the charged pion and longitudinal rho meson from the diagonal Landau-projected kernels. As shown in Fig.1, both  $E_\pi(B)$  and  $E_\rho(B)$  increase monotonically with magnetic field and exhibit the expected  $\sqrt{eB}$  behavior at large fields, reflecting Landau quantization. When converted to rest masses via  $m_\phi = \sqrt{E_\phi^2 - eB}$ , the charged pion mass remains monotonic. The strict monotonicity of the unmixed LLL energies

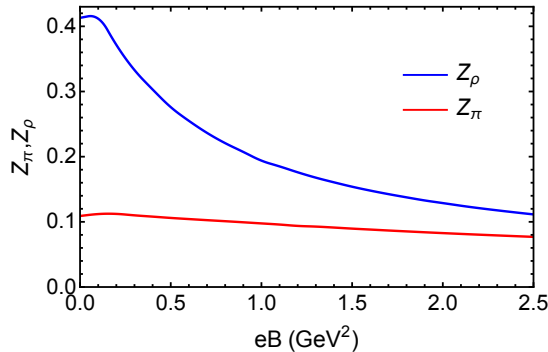


FIG. 2: Wave-function renormalizations  $Z_\pi(B)$  and  $Z_\rho(B)$  extracted from the slopes of the diagonal LLL Landau-projected kernels at the poles. While  $Z_\pi(B)$  decreases mildly with increasing magnetic field,  $Z_\rho(B)$  is rapidly suppressed in the LLL.

demonstrates that Landau quantization and magnetic catalysis alone cannot generate a turnover.

The wave-function renormalizations extracted from the near-pole slopes are shown in Fig.2. A crucial feature is the qualitatively different magnetic-field dependence in the two channels. While  $Z_\pi(B)$  decreases mildly,  $Z_\rho(B)$  is rapidly suppressed in the LLL and becomes very small at strong fields. Physically, the suppression of  $Z_\rho(B)$  reflects the restructuring of the longitudinal vector correlator in a magnetic background, where the tensor decomposition reduces the spectral weight carried by the pole. The collapse of  $Z_\rho(B)$  dynamically amplifies mixing effects near the pole.

The loop-induced mixing coupling  $g_{\rho\pi}^{\text{loop}}(B)$ , defined in (11), is shown in the upper panel of Fig.3 and evaluated at  $q_0 = E_\pi(B)$ . The loop contribution encodes infrared quark dynamics in a magnetic field and is smaller than the tree-level term fixed by the vacuum decay  $\rho^\pm \rightarrow \pi^\pm + \gamma$ , as expected in an EFT description. The total mixing strength  $h(B)$ , shown in the lower panel, grows strongly with increasing magnetic field. Although  $g_{\rho\pi}^{\text{loop}}(B)$  alone decreases with  $B$ , the total mixing is enhanced by the explicit  $eB$  factor and, more importantly, by the suppression of  $Z_\rho(B)$  in the denominator. The effective near-pole mixing is therefore dynamically amplified even when the microscopic loop contribution remains moderate.

Solving the pole condition (2) yields two mixed eigenmodes. The lower eigenmode  $E_-$  is shown in Fig.4. At weak fields it closely follows the unmixed pion LLL energy. At intermediate fields, increasing mixing induces level repulsion between the light pion mode and the heavier longitudinal rho mode, causing the lower eigenvalue to bend downward. This turnover is a direct consequence of residue-enhanced pion-rho mixing within the same Landau level. For comparison, Fig.4 also shows the result obtained by solving  $\det \mathcal{K}(q_0) = 0$  directly using the full Landau-level-projected kernel (9). At weak and intermediate fields the two approaches agree, confirming that the

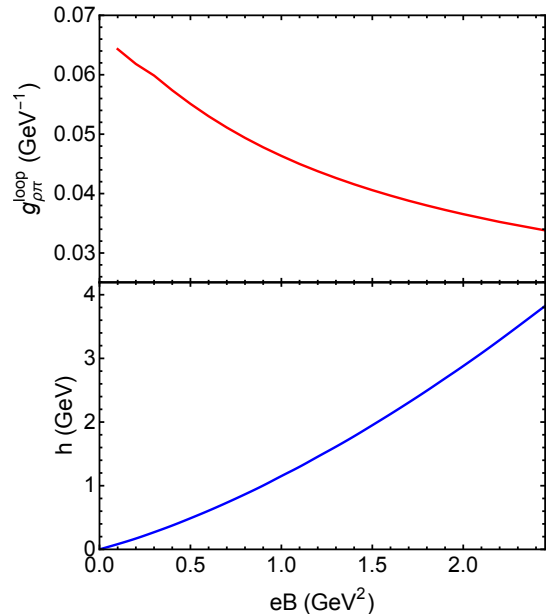


FIG. 3: Upper panel: Loop-induced mixing coupling  $g_{\rho\pi}^{\text{loop}}(B)$  defined in (11), evaluated at  $q_0 = E_\pi(B)$ . Lower panel: Total mixing strength  $h(B)$  defined in (4), including both loop-induced and tree-level contributions.

near-pole formulation captures the essential determinant physics. At larger  $eB$  the increasing deviation reflects sensitivity to higher-order energy dependence and provides a quantitative estimate of systematic uncertainties in the truncated near-pole description.

Lattice simulations extract an effective mass from the long-time behavior of charged-pion correlators, corresponding to the lowest physical eigenmode rather than to the unmixed pion Landau level. The nonmonotonic behavior obtained here—rising at small magnetic fields, reaching a maximum at intermediate fields, and decreasing at larger fields—qualitatively reproduces this observation. For orientation, the vertical lines in Fig.4 indicate the characteristic field strengths identified in lattice simulations: the onset of deviation from simple LLL behavior around  $eB \simeq 0.3 \text{ GeV}^2$  and the location of the maximal effective mass near  $eB \simeq 0.6\text{--}0.7 \text{ GeV}^2$ . The direct determinant solution shifts the maximum toward smaller  $eB$  compared with the near-pole truncation, indicating that higher-order energy dependence further enhances the same mixing mechanism. The turnover therefore emerges robustly at the level of determinant dynamics, even though its precise location depends on quantitative details of the kernel.

While the precise location of the maximum depends on quantitative details such as the magnetic-field dependence of  $Z_\rho(B)$  and the effective pion-rho coupling, the existence of the turnover does not rely on fine tuning. In the near-pole framework, it is controlled by the competition between Landau-level separation and residue-

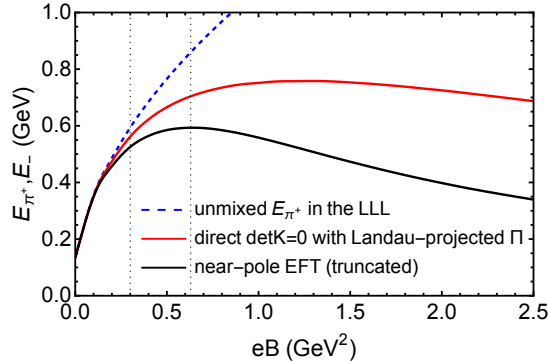


FIG. 4: Lowest eigenmode of the coupled  $\pi^+ - \rho_{s_z=0}^+$  system in the lowest Landau level as a function of the magnetic field. The dashed blue curve shows the unmixed pion LLL energy  $E_{\pi^+}$ . The red curve corresponds to the lower eigenmode  $E_-$  obtained from the near-pole effective kernel (1), while the black curve is obtained by solving  $\det \mathcal{K}(q_0) = 0$  directly using the Landau-level-projected kernel (9), without invoking the near-pole expansion. The vertical lines at  $eB \simeq 0.3$   $\text{GeV}^2$  and  $eB \simeq 0.65$   $\text{GeV}^2$  indicate the characteristic field strengths where lattice simulations observe the onset of deviation from lowest-Landau-level behavior and the location of the maximal effective mass, respectively.

enhanced mixing. Corrections beyond the present treatment—such as nonlocal interactions or continuum effects in the polarization functions—may shift the peak position without altering the underlying mechanism.

We have also tested the sensitivity of the turnover to a constant rho width implemented via  $q_0 \rightarrow q_0 + i\Gamma_\rho/2$  in the diagonal near-pole kernel. For moderate widths  $\Gamma_\rho \sim 0.2$   $\text{GeV}$  the peak position changes only mildly, while substantial shifts require  $\Gamma_\rho$  of order 1  $\text{GeV}$ . This indicates that the turnover is not controlled by a naive constant damping term, but primarily by the magnetic-field dependence of near-pole residues and mixing.

*Summary and Discussion* In this Letter, we have identified a clean microscopic mechanism underlying the non-monotonic magnetic-field dependence of the charged pion mass observed in lattice QCD. Starting from a quark-level description and formulating the problem in terms of Landau-projected near-pole dynamics, we showed that the lowest-Landau-level charged pion mixes with the longitudinally polarized charged rho meson in a magnetic background. This symmetry-allowed mixing induces level repulsion, which is dynamically amplified by a rapid suppression of the rho-meson wave-function renormalization near the pole. The resulting residue-enhanced mixing drives the downward bending of the lower eigenmode at strong magnetic fields.

A central implication of this analysis is that, in the presence of strong mixing, lattice observables are governed by the lowest near-pole eigenmode rather than

by unmixed Landau levels or rest-mass shifts alone. Residue effects—typically subleading in vacuum spectroscopy—become decisive in magnetic backgrounds.

The near-pole extraction scheme provides a canonically normalized and physically transparent description of the collective modes, but it relies on the assumption that the physical eigenmode remains adiabatically connected to the unmixed LLL pole. At sufficiently large magnetic fields, where mixing becomes strong, this approximation gradually loses accuracy. This limitation is directly reflected in Fig.4 by the separation between the near-pole eigenmode and the direct solution of  $\det \mathcal{K}(q_0) = 0$ . The nonmonotonic behavior itself, however, remains robust at the level of the full determinant dynamics.

While the precise location of the maximum depends on quantitative details such as the magnetic-field dependence of the rho residue and the effective  $\pi - \rho$  coupling, the existence of the turnover requires only the coexistence of Landau quantization, symmetry-allowed mixing, and strongly field-dependent residues. The mechanism therefore does not rely on fine tuning and is expected to be generic for charged mesons in strong magnetic fields.

More broadly, the framework developed here provides a controlled starting point for extending such analyses to other mesonic systems. In the light sector, mixing with axial-vector modes represents a natural next step. For strange mesons, pseudoscalar–vector mixing remains symmetry-allowed but is moderated by flavor-symmetry breaking, suggesting a weaker nonmonotonic behavior. In heavy-flavor systems, magnetic-field-induced mixing persists in principle but is parametrically suppressed by heavy-quark spin symmetry. This hierarchy highlights the special role of chiral dynamics in the pion sector and delineates the regime of applicability of the present mechanism.

## ACKNOWLEDGMENTS

The author would like to thank Pengfei Zhuang for fruitful discussion. The work is supported by NSFC grant Nos. 12005112 and The Fundamental Research Funds for Beijing Municipal Universities.

## Appendix A: Landau projected polarization function

The polarization function projected to the lowest Landau level meson states are given by

$$\begin{aligned}\Pi_{\pi\pi,0} &= -\frac{4N_c e B}{3\pi} \int \frac{dk_3}{(2\pi)} \sum_{i,j=0}^{\infty} \left[ Y_1(i,j) I_3(q_0) \right. \\ &\quad \left. + \left( (k_3^2 + m^2) Y_1(i,j) + \frac{8}{3l^2} Y_2(i,j) \right) I_2(q_0) \right], \\ \Pi_{\rho\rho,0} &= -\frac{4N_c e B}{3\pi} \int \frac{dk_3}{(2\pi)} \sum_{i,j=0}^{\infty} \left[ Y_1(i,j) I_3(q_0) \right. \\ &\quad \left. + \left( (-k_3^2 + m^2) Y_1(i,j) + \frac{8}{3l^2} Y_2(i,j) \right) I_2(q_0) \right], \\ \Pi_{\rho\pi,0}^3 &= -(-im_f q_0) \frac{4N_c e B}{3\pi} \int \frac{dk_3}{(2\pi)} \sum_{i,j=0}^{\infty} Y_3(i,j) I_2(q_0), \\ \Pi_{\pi\rho,0}^3 &= -(+im_f q_0) \frac{4N_c e B}{3\pi} \int \frac{dk_3}{(2\pi)} \sum_{i,j=0}^{\infty} Y_3(i,j) I_2(q_0).\end{aligned}$$

These expressions are evaluated numerically after Pauli–Villars regularization and summation over Landau levels up to  $n = 200$  and sufficient corresponding  $m$ . The

functions  $I_2(q_0)$  and  $I_3(q_0)$  encodes the Matsubara sum,

$$\begin{aligned}I_2 &= \frac{1}{4E_{u,i}E_{d,j}} \left( \frac{n_F(E_{d,j}) - n_F(E_{u,i})}{(E_{d,j} - E_{u,i} + q_0)} + \frac{n_F(E_{d,j}) - n_F(E_{u,i})}{(E_{d,j} - E_{u,i} - q_0)} \right. \\ &\quad \left. + \frac{1 - n_F(E_{d,j}) - n_F(E_{u,i})}{(E_{d,j} + E_{u,i} - q_0)} + \frac{1 - n_F(E_{d,j}) - n_F(E_{u,i})}{(E_{d,j} + E_{u,i} + q_0)} \right), \\ I_3 &= \frac{1}{4} \left( \frac{n_F(E_{d,j}) - n_F(E_{u,i})}{(-E_{d,j} + E_{u,i} - q_0)} + \frac{n_F(E_{d,j}) - n_F(E_{u,i})}{(-E_{d,j} + E_{u,i} + q_0)} \right. \\ &\quad \left. + \frac{1 - n_F(E_{d,j}) - n_F(E_{u,i})}{(E_{d,j} + E_{u,i} - q_0)} + \frac{1 - n_F(E_{d,j}) - n_F(E_{u,i})}{(E_{d,j} + E_{u,i} + q_0)} \right),\end{aligned}$$

with  $E_{u,i}^2 = 2i|q_u B| + k_3^2 + m_f^2$  and  $E_{d,j}^2 = 2j|q_d B| + k_3^2 + m_f^2$ . The coefficients  $Y_i$  are defined as

$$\begin{aligned}Y_1(m, n) &= -\frac{2^{m-1}}{3^{n+m}} \frac{(m+2n)\Gamma(n+m)}{\Gamma(1+n)\Gamma(1+m)}, \\ Y_2(m, n) &= -\frac{2^{m-1}}{3^{n+m}} \frac{\Gamma(n+m)}{\Gamma(n)\Gamma(m)}, \\ Y_3(n, m) &= -\frac{2^{m-1}}{3^{n+m}} \frac{(m-2n)\Gamma(n+m)}{\Gamma(1+n)\Gamma(1+m)}.\end{aligned}$$

---

[1] Dario Grasso and Hector R. Rubinstein. Magnetic fields in the early universe. *Phys. Rept.*, 348:163–266, 2001.

[2] Ruth Durrer and Andrii Neronov. Cosmological Magnetic Fields: Their Generation, Evolution and Observation. *Astron. Astrophys. Rev.*, 21:62, 2013.

[3] Kenta Kiuchi, Pablo Cerdá-Durán, Koutarou Kyutoku, Yuichiro Sekiguchi, and Masaru Shibata. Efficient magnetic-field amplification due to the Kelvin-Helmholtz instability in binary neutron star mergers. *Phys. Rev. D*, 92(12):124034, 2015.

[4] V. Skokov, A. Yu. Illarionov, and V. Toneev. Estimate of the magnetic field strength in heavy-ion collisions. *Int. J. Mod. Phys. A*, 24:5925–5932, 2009.

[5] Wei-Tian Deng and Xu-Guang Huang. Event-by-event generation of electromagnetic fields in heavy-ion collisions. *Phys. Rev. C*, 85:044907, 2012.

[6] Dmitri E. Kharzeev, Larry D. McLerran, and Harmen J. Warringa. The Effects of topological charge change in heavy ion collisions: 'Event by event P and CP violation'. *Nucl. Phys. A*, 803:227–253, 2008.

[7] Dmitri E. Kharzeev and Dam T. Son. Testing the chiral magnetic and chiral vortical effects in heavy ion collisions. *Phys. Rev. Lett.*, 106:062301, 2011.

[8] Umut Gursoy, Dmitri Kharzeev, and Krishna Rajagopal. Magnetohydrodynamics, charged currents and directed flow in heavy ion collisions. *Phys. Rev. C*, 89(5):054905, 2014.

[9] V. P. Gusynin, V. A. Miransky, and I. A. Shovkovy. Dimensional reduction and catalysis of dynamical symmetry breaking by a magnetic field. *Nucl. Phys. B*, 462:249–290, 1996.

[10] Dmitri E. Kharzeev and Ho-Ung Yee. Chiral Magnetic Wave. *Phys. Rev. D*, 83:085007, 2011.

[11] G. S. Bali, F. Bruckmann, G. Endrodi, Z. Fodor, S. D. Katz, and A. Schafer. QCD quark condensate in external magnetic fields. *Phys. Rev. D*, 86:071502, 2012.

[12] Akio Tomiya, Heng-Tong Ding, Xiao-Dan Wang, Yu Zhang, Swagato Mukherjee, and Christian Schmidt. Phase structure of three flavor QCD in external magnetic fields using HISQ fermions. *PoS, LATTICE2018:163*, 2019.

[13] G. S. Bali, F. Bruckmann, G. Endrödi, S. D. Katz, and A. Schäfer. The QCD equation of state in background magnetic fields. *JHEP*, 08:177, 2014.

[14] G. S. Bali, F. Bruckmann, M. Constantinou, M. Costa, G. Endrodi, S. D. Katz, H. Panagopoulos, and A. Schafer. Magnetic susceptibility of QCD at zero and at finite temperature from the lattice. *Phys. Rev. D*, 86:094512, 2012.

[15] Vladimir A. Miransky and Igor A. Shovkovy. Quantum field theory in a magnetic field: From quantum chromodynamics to graphene and Dirac semimetals. *Phys. Rept.*, 576:1–209, 2015.

[16] Kenji Fukushima and Yoshimasa Hidaka. Magnetic Catalysis Versus Magnetic Inhibition. *Phys. Rev. Lett.*, 110(3):031601, 2013.

[17] Jens O. Andersen, William R. Naylor, and Anders Tranberg. Phase diagram of QCD in a magnetic field: A review. *Rev. Mod. Phys.*, 88:025001, 2016.

[18] G. S. Bali, F. Bruckmann, G. Endrodi, Z. Fodor, S. D. Katz, S. Krieg, A. Schafer, and K. K. Szabo. The QCD phase diagram for external magnetic fields. *JHEP*, 02:044, 2012.

[19] E. M. Ilgenfritz, M. Müller-Preussker, B. Petersson, and A. Schreiber. Magnetic catalysis (and inverse catalysis) at finite temperature in two-color lattice QCD. *Phys. Rev. D*, 89(5):054512, 2014.

[20] H. T. Ding, S. T. Li, A. Tomiya, X. D. Wang, and Y. Zhang. Chiral properties of (2+1)-flavor QCD in strong magnetic fields at zero temperature. *Phys. Rev. D*, 104(1):014505, 2021.

[21] Heng-Tong Ding, Sheng-Tai Li, Swagato Mukherjee, Akio Tomiya, and Xiao-Dan Wang. Meson masses in external magnetic fields with HISQ fermions. *PoS, LATICE2019:250*, 2020.

[22] Heng-Tong Ding and Dan Zhang. Chiral Properties of (2+1)-Flavor QCD in Magnetic Fields at Zero Temperature. 1 2026.

[23] Tomohiro Inagaki, Daiji Kimura, and Tsukasa Murata. Four fermion interaction model in a constant magnetic field at finite temperature and chemical potential. *Prog. Theor. Phys.*, 111:371–386, 2004.

[24] Lang Yu, Jos Van Doorsselaere, and Mei Huang. Inverse Magnetic Catalysis in the three-flavor NJL model with axial-vector interaction. *Phys. Rev. D*, 91(7):074011, 2015.

[25] Sh. Fayazbakhsh and N. Sadooghi. Anomalous magnetic moment of hot quarks, inverse magnetic catalysis, and reentrance of the chiral symmetry broken phase. *Phys. Rev. D*, 90(10):105030, 2014.

[26] M. Coppola, D. Gómez Dumm, and N. N. Scoccola. Charged pion masses under strong magnetic fields in the NJL model. *Phys. Lett. B*, 782:155–161, 2018.

[27] M. Coppola, D. Gomez Dumm, S. Noguera, and N. N. Scoccola. Neutral and charged pion properties under strong magnetic fields in the NJL model. *Phys. Rev. D*, 100(5):054014, 2019.

[28] Nilanjan Chaudhuri, Snigdha Ghosh, Sourav Sarkar, and Pradip Roy. Effect of the anomalous magnetic moment of quarks on the phase structure and mesonic properties in the NJL model. *Phys. Rev. D*, 99(11):116025, 2019.

[29] Kazuhiko Kamikado and Takuya Kanazawa. Chiral dynamics in a magnetic field from the functional renormalization group. *JHEP*, 03:009, 2014.

[30] Kiminad A. Mamo. Inverse magnetic catalysis in holographic models of QCD. *JHEP*, 05:121, 2015.

[31] Danning Li, Mei Huang, Yi Yang, and Pei-Hung Yuan. Inverse Magnetic Catalysis in the Soft-Wall Model of AdS/QCD. *JHEP*, 02:030, 2017.

[32] Sidney S. Avancini, Máximo Coppola, Norberto N. Scoccola, and Joana C. Sodré. Light pseudoscalar meson masses under strong magnetic fields within the SU(3) Nambu–Jona-Lasinio model. *Phys. Rev. D*, 104(9):094040, 2021.

[33] J. P. Carlomagno, D. Gomez Dumm, M. F. Izzo Vilafañe, S. Noguera, and N. N. Scoccola. Charged pseudoscalar and vector meson masses in strong magnetic fields in an extended NJL model. *Phys. Rev. D*, 106(9):094035, 2022.

[34] Máximo Coppola, Daniel Gomez Dumm, Santiago Noguera, and Norberto N. Scoccola. Masses of magnetized pseudoscalar and vector mesons in an extended NJL model: The role of axial vector mesons. *Phys. Rev. D*, 109(5):054014, 2024.

[35] Rui Wen, Shi Yin, Wei-jie Fu, and Mei Huang. Functional renormalization group study of neutral and charged pions in magnetic fields in the quark-meson model. *Phys. Rev. D*, 108(7):076020, 2023.

[36] Luyang Li and Shijun Mao. Inverse magnetic catalysis effect and current quark mass effect on mass spectra and Mott transitions of pions under external magnetic field. *Phys. Rev. D*, 108(5):054001, 2023.

[37] Hao Liu, Lang Yu, and Mei Huang. Charged and neutral vector  $\rho$  mesons in a magnetic field. *Phys. Rev. D*, 91(1):014017, 2015.

[38] Snigdha Ghosh, Arghya Mukherjee, Mahatsab Mandal, Sourav Sarkar, and Pradip Roy. Spectral properties of  $\rho$  meson in a magnetic field. *Phys. Rev. D*, 94(9):094043, 2016.

[39] Mamiya Kawaguchi and Shinya Matsuzaki. Vector meson masses from a hidden local symmetry in a constant magnetic field. *Phys. Rev. D*, 93(12):125027, 2016.

[40] S. P. Klevansky. The Nambu–Jona-Lasinio model of quantum chromodynamics. *Rev. Mod. Phys.*, 64:649–708, 1992.

[41] Tetsuo Hatsuda and Teiji Kunihiro. QCD phenomenology based on a chiral effective Lagrangian. *Phys. Rept.*, 247:221–367, 1994.

[42] U. Vogl and W. Weise. The Nambu and Jona Lasinio model: Its implications for hadrons and nuclei. *Prog. Part. Nucl. Phys.*, 27:195–272, 1991.

[43] Julian S. Schwinger. On gauge invariance and vacuum polarization. *Phys. Rev.*, 82:664–679, 1951.